Supplementary Information

Single-Molecule Spectroscopy Reveals the Plasmon-Assisted Nanozyme Catalysis on AuNR@TiO_2

Li Zuo[†‡], Hallie King[†], Mohammad Akter Hossain[†], Fatiha Farhana[†], Madelyn M. Kist[†], Rebecca L. Stratton[†], Jiao Chen[†], Hao Shen[†*]

* Corresponding Author: hshen7@kent.edu

Table of Contents

Materials.

All experiments were carried out using commercial reagents without further purifications. The colloidal gold nanorods (25 nm × 75 nm) were purchased from Nanopartz (A12-25-700). The stock $TiCl_3$ (10-15% basis, 14010) and sodium bicarbonate ($NaHCO_3$, S6014) were obtained from Sigma-Aldrich. 30% hydrogen peroxide (H_2O_2, H1070) and 2.0 N hydrochloric acid (18-603-172) were purchased from Spectrum Chemical Corp. The fluorogenic probe, Amplex Red reagent (A12222), with a purity of at least 95%, was purchased from Invitrogen. Prior to conducting the single-molecule experiments, AR was dissolved in 50 mM, pH 7.4 phosphate buffer.

Synthesis and characterization of AuNR@TiO_2 nanozymes.

For the synthesis, 0.2 mL $TiCl_3$ stock solution was diluted by adding 5 mL DI-water, which had been degassed after 5 min sonication. Subsequently, ~1 mL 1 M $NaHCO_3$ solution was added dropwise to the $TiCl_3$ solution under continuous stirring. It is worth noting that the terminal stage of $NaHCO_3$ addition is crucial to the synthesis: the last one or two drops could rapidly transform the mixture into a dark blue color. This sudden color shift reflects the pH change of the solution. The resulting solution is expected to have a final pH ~2.5.

After adjusting the pH of the Ti^{3+} precursor, 2 mL AuNR stock solution was added, and the mixture was gently stirred for 1 hour. Following this, the nanozymes were isolated through

centrifugation at a speed of 5,000 rpm for 2 minutes. The collected nanozymes were then washed with diluted H_2O_2 solution (~5 mM) four times and then re-dispersed into 1 mL DI-H_2O.

Transmission electron microscopy (TEM).

All the samples were diluted to a concentration of 10 pM for TEM imaging. Subsequently, 2 μL of the suspended sample was drop-casted onto 200-mesh carbon-coated copper grids (Ted Pella, catalog #01840). The grids were left in air for ~2 hours to allow the solvent to evaporate. The TEM images were acquired using a FEI Tecnai G2 F20 that operated at 250 kV. Additionally, Energy-Dispersive X-ray (EDX) spectroscopy was conducted, utilizing a coupled detector for elemental analysis.

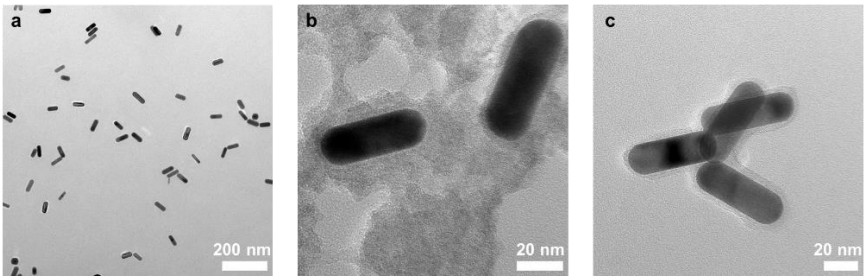

Figure S1. TEM images of as-received AuNRs (a), prepared AuNRs@TiO_2 before rinsing (b) and after rinsing (c).

The TEM images for as-received AuNRs and AuNRs@TiO_2 are shown in **Fig. S1**. Before rinsing, weakly bound amorphous TiO_2 remained next to the AuNRs@TiO_2 (**Fig. S1b**). These weakly bound TiO_2 were sufficiently removed after rinsing (**Fig. S1c**). The EDX spectrum for nanozymes shown in **Fig. S1c** confirmed the successful deposition of TiO_2 shell surrounding AuNR, evidenced by a clear Ti peak in **Fig. S2**.

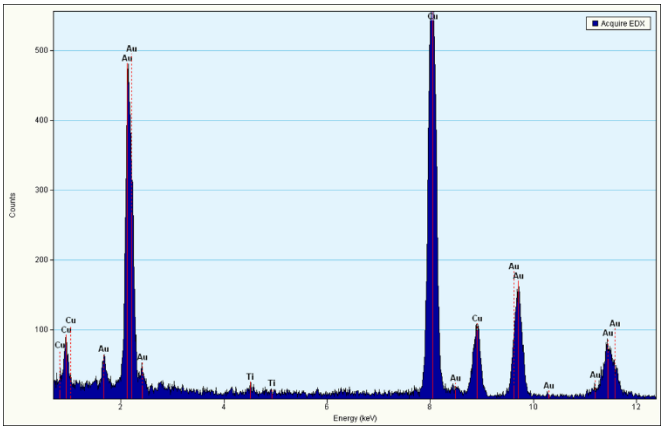

Figure S2. EDX elementary analysis. The detector is focused on the rinsed AuNRs@TiO_2 nanozymes.

The size and aspect ratio distributions for both pristine AuNRs and AuNR@TiO_2 nanozymes are shown in **Fig. S3a** and **b**. Our statistics (220 AuNRs and 70 AuNRs@TiO_2) indicate that the as-received AuNRs are 18 × 54 nm. Notably, the successive synthesis steps

exhibited no discernible influence on the observable sizes of the AuNRs. The aspect ratio remained at 2.8 after TiO_2 coating. It was found that the TiO_2 shell was mostly amorphous because it was synthesized at room temperature without subsequent thermal annealing. The embedded Au lattice with the distance of ~0.23 nm inside the TiO_2 shell reflected the relatively strong interaction between these two components (**Fig. S3c, inset**). The thickness of TiO_2 layer was estimated to be 3.0 ± 0.1 nm using 38 AuNR@TiO_2 nanozymes (**Fig. S3d**).

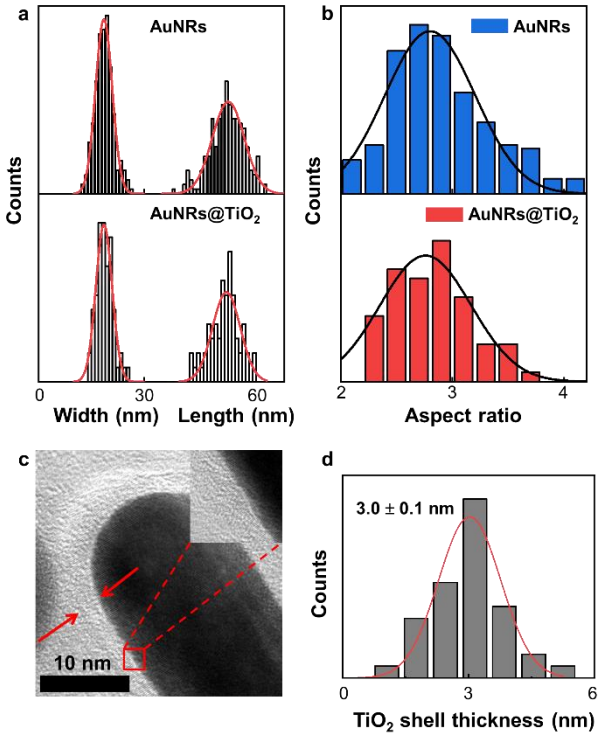

Figure S3. (a) Size distributions for AuNR and AuNR@TiO_2 nanozymes. (b) Aspect ratio distributions for AuNR and AuNR@TiO_2 nanozymes. (c) High-resolution TEM image of one AuNR@TiO_2. Red arrows mark out the thin TiO_2 shell. Inset: The zoom-in image of the boxed region. (d) Distribution of the TiO_2 shell thickness.

UV-Vis spectrum.

The UV-Vis spectra for the dispersed AuNRs and AuNR@TiO_2 nanozymes were recorded by an Agilent Cary60 spectrophotometer (**Fig. 2a** in the main text). The longitudinal and transverse SPR for pristine AuNRs were determined to be 685 and 517 nm, respectively. After the TiO_2 coating, discernible red shifts occurred for SPR bands, further supporting the formation of TiO_2 shell on AuNR. In particular, the longitudinal SPR was severely inhibited. These discernible shifts were likely due to the local refractive index change surrounding the AuNRs, as discussed in previous studies[1-3].

Fluorogenic probing reaction.

The N-deacetylation of AR oxidation, a typical fluorogenic reaction for peroxidase[4, 5], was used to test the catalytic performance of AuNRs and AuNRs@TiO_2 nanozymes. This reaction yields the high fluorescence molecule resorufin (RF) at a 1:1 stoichiometric ratio. The ensemble catalysis was performed by measuring the fluorescence spectra in an Agilent Cary60

fluorometer. Solutions of 20 μM AR and 60 mM H_2O_2 solutions were pre-mixed in a 50 mM pH 7.4 phosphate buffer. To initiate the catalytic transformation, 50 pM nanoparticles were added to the reaction mixture. The formation of RFs was evidenced by the increasing fluorescence intensity peaking at 583 nm (**Fig 1d** in the main text). The AR → RF conversion is a pseudo-first order reaction; the fluorescence intensity increased linearly to the reaction time because of the relatively slow reaction rate. Hence, we used the slopes of the intensity-time trajectories for reactivity comparison.

It is well known that TiO_2 is a commonly used catalyst for many oxidation reactions[6-9]. To rule out the chemical and photochemical reactivity from pure TiO_2, we performed control experiments on pristine AuNRs, AuNRs@TiO_2 and commercial TiO_2 (a rutile and anatase mixture) with and without 530 nm LED excitation (**Fig. S4a**). It was found that commercial TiO_2 barely exhibited any reactivity even with the 530 nm LED excitation. Strikingly, the reactivity of AuNRs@TiO_2 increased ~tenfold with the addition of 530 nm LED, demonstrating considerable SPR enhancement. Moreover, the addition of a 700 nm LED did not significantly improve the reactivity of AuNRs@TiO_2 likely due to decreased absorbance under this wavelength after TiO_2 deposition (**Fig S4b**). The reactivity of synthesized TiO_2 before and after oxidation treatment was measured, as shown in **Fig. S4c**. The freshly prepared TiO_2 exhibited high reactivity due to the existence of residual Ti(III) defective sites. By washing the sample using H_2O_2, majority of the Ti(III) sites were oxidized, resulting in the decrease of the TiO_2 reactivity.

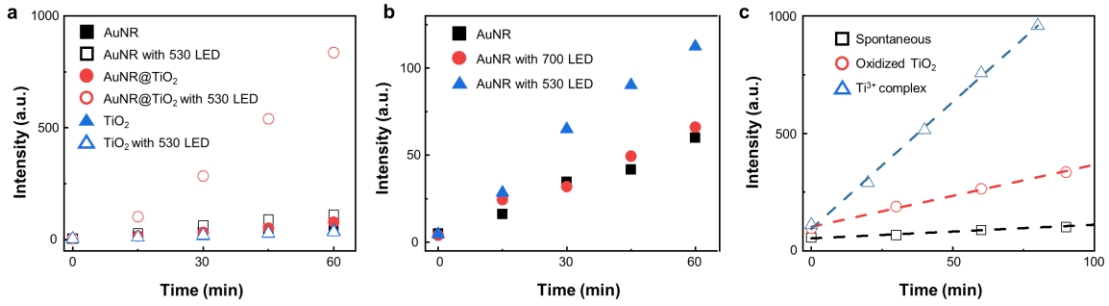

Figure S4. Ensemble reactivity for AR oxidation. (a) The time-evolving fluorescence intensity at 583 nm for AuNR, AuNR@TiO_2 and TiO_2 with and without the 530 nm LED illumination. (b) The time-evolving fluorescence intensity on AuNR with 530 nm and 700 nm LED illumination. (c) Comparison between the reactivity of TiO_{2-x} before and after oxidation treatment.

Single-molecule data analysis.

The data analysis of the recorded movie was achieved using ThunderSTORM[10, 11] and a home-written Matlab program, which was detailed in our previous work[12]. Briefly, the analysis contained three major steps: (1) Identifying single RF molecules in each frame and fitting their emission signals to 2D Gaussian functions to extract the centroid localizations. This step is accomplished by ThunderSTORM. (2) Correctly assign the centroids of RF molecules to their parent nanozymes, based on the nearest-neighbor algorithm by a Matlab program. (3) Extract individual waiting time τ for each nanozyme by calculating the duration between two consecutive RF molecules. This step is accomplished by another homemade Matlab program.

A full catalytic turnover within a single nanozyme encompasses two critical waiting periods, τ_{off} and τ_{on}. τ_{off} refers to the interval following the disappearance of a fluorescence spike and preceding the emergence of the next spike, while τ_{on} pertains to the period a fluorescent product remains visible until it vanishes. τ_{off} is associated with the catalytic conversion of the reactant molecule, and τ_{on} correlates with the product molecule's desorption. The combination of τ_{on} and τ_{off} constitutes the turnover time, τ. Given that τ_{on} (approximately 100 milliseconds) is significantly shorter than τ_{off} (spanning tens of seconds), τ is essentially equivalent to τ_{off}. Consequently, we focused on analyzing $<\tau>^{-1}$ in this study as an effective approximation.

Stability of AuNR@TiO_2.

Though the catalytic reactivity of individual nanozyme fluctuates, the average reactivity of AuNR@TiO_2 remained stable in the experiments with a duration of ~8 hours (**Fig. S5**). This result suggests that the AuNR@TiO_2 nanozymes remained stable during our measurements.

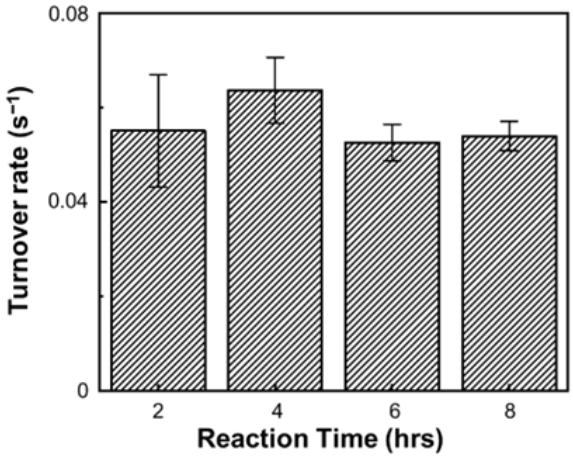

Figure S5. Stability of AuNR@TiO_2. The averaged reactivity for the same batch of nanozymes was measured after 2 hours, 4 hours, 6 hours and 8 hours of reaction. [AR] = 800 nM, [H_2O_2] = 60 mM in 50 mM pH7.4 phosphate buffer.

Catalytic kinetics model.

The Michaelis-Menten mechanism is a common model to describe the kinetics in enzyme catalysis[13-16]. In this mechanism, a substrate binds to an enzyme to form an enzyme-substrate complex and then converts to the product molecule[14, 16]. The reaction rate v is expressed as:

$$v = \frac{k_{\mathrm{cat}}[E][S]}{K_{\mathrm{M}} + [S]}$$

where k_{cat} is the catalytic rate constant, $[E]$ the total concentration of enzyme, K_M the Michaelis constant, and $[S]$ the substrate concentration. In classic Michaelis-Menten mechanism, it assumes that the catalyst, enzyme, only has one reactive site and convert the substrate molecule one by one. However, the prepared AuNR@TiO_2 nanozymes contain multiple reactive sites. Furthermore, the enzyme concentration $[E]$ becomes meaningless at single-molecule level because only one enzyme is studied. Therefore, we used the modified Michaelis-Menten

equation (**Eq 1** in the main text) to describe the catalytic kinetics. Compared to the classic Michaelis-Menten mechanism, this modified equation assumes n reactive sites available on the nanozymes with the single site rate constant equals to k_{cat}. The Michaelis constant K_M reflects the binding affinity between the substrates and the reactive sites. The apparent reaction rate ν, on a single nanozyme is seen as the inverse average of reaction waiting time $<\tau>^{-1}$, which is readily observable from our measurement.

Reference.

(1) Ding, D.; Liu, K.; He, S.; Gao, C.; Yin, Y. Ligand-exchange assisted formation of Au/TiO_2 Schottky contact for visible-light photocatalysis. *Nano Lett* **2014**, *14* (11), 6731-6736.

(2) Ngaw, C. K.; Xu, Q.; Tan, T. T. Y.; Hu, P.; Cao, S.; Loo, J. S. C. A strategy for in-situ synthesis of well-defined core–shell Au@TiO_2 hollow spheres for enhanced photocatalytic hydrogen evolution. *Chemical Engineering Journal* **2014**, *257*, 112-121.

(3) Wu, B.; Liu, D.; Mubeen, S.; Chuong, T. T.; Moskovits, M.; Stucky, G. D. Anisotropic Growth of TiO_2 onto Gold Nanorods for Plasmon-Enhanced Hydrogen Production from Water Reduction. *J Am Chem Soc* **2016**, *138* (4), 1114-1117.

(4) Shen, H.; Zhou, X.; Zou, N.; Chen, P. Single-Molecule Kinetics Reveals a Hidden Surface Reaction Intermediate in Single-Nanoparticle Catalysis. *J. Phys. Chem. C* **2014**, *118* (46), 26902-26911.

(5) Zhou, X.; Andoy, N. M.; Liu, G.; Choudhary, E.; Han, K. S.; Shen, H.; Chen, P. Quantitative super-resolution imaging uncovers reactivity patterns on single nanocatalysts. *Nat Nanotechnol* **2012**, *7* (4), 237-241.

(6) Martin Setvín, U. A., Philipp Scheiber, YeFei Li, Weiyi Hou, Michael Schmid, Annabella Selloni, Ulrike Diebold. Reaction of O_2 with Subsurface Oxygen Vacancies on TiO_2 Anatase (101). *Science* **2013**, *341* (30), 988-991.

(7) Pan, X.; Yang, M. Q.; Fu, X.; Zhang, N.; Xu, Y. J. Defective TiO_2 with oxygen vacancies: synthesis, properties and photocatalytic applications. *Nanoscale* **2013**, *5* (9), 3601-3614.

(8) Wang, Z.; Yang, C.; Lin, T.; Yin, H.; Chen, P.; Wan, D.; Xu, F.; Huang, F.; Lin, J.; Xie, X.; et al. H-Doped Black Titania with Very High Solar Absorption and Excellent Photocatalysis Enhanced by Localized Surface Plasmon Resonance. *Advanced Functional Materials* **2013**, *23* (43), 5444-5450.

(9) Lang, X.; Chen, X.; Zhao, J. Heterogeneous visible light photocatalysis for selective organic transformations. *Chem Soc Rev* **2014**, *43* (1), 473-486.

(10) Bo Huang, W. W., Mark Bates, Xiaowei Zhuang. Three-Dimensional Super-Resolution Imaging by Stochastic Optical Reconstruction Microscopy. *Science* **2008**, *319* (8), 810-813.

(11) Ovesny, M.; Krizek, P.; Borkovec, J.; Svindrych, Z.; Hagen, G. M. ThunderSTORM: a comprehensive ImageJ plug-in for PALM and STORM data analysis and super-resolution imaging. *Bioinformatics* **2014**, *30* (16), 2389-2390.

(12) Zuo, L.; Ren, K.; Guo, X.; Pokhrel, P.; Pokhrel, B.; Hossain, M. A.; Chen, Z. X.; Mao, H.; Shen, H. Amalgamation of DNAzymes and Nanozymes in a Coronazyme. *J Am Chem Soc* **2023**, *145* (10), 5750-5758.

(13) Doka, E.; Lente, G. Stochastic mapping of the Michaelis-Menten mechanism. *J Chem Phys*

2012, *136* (5), 054111.
(14) Weilin Xu, J. S. K., Peng Chen. Single-Molecule Kinetic Theory of Heterogeneous and Enzyme Catalysis *J. Phys. Chem. C* **2009**, *113* (6), 2393-2404.
(15) Chaudhury, S.; Cherayil, B. J. Dynamic disorder in single-molecule Michaelis-Menten kinetics: the reaction-diffusion formalism in the Wilemski-Fixman approximation. *J Chem Phys* **2007**, *127* (10), 105103.
(16) S. C. Kou, B. J. C., Wei Min, Brian P. English, X. Sunney Xie. Single-Molecule Michaelis-Menten Equations. *J. Phys. Chem. B* **2005**, *109* (41), 19068-19081.